Research Article

Journal of Environmental Nanotechnology

pH-Tuned Synthesis of Samarium-Doped MoO_3/SiO_2 Nanocomposite for Enhanced Electrochemical Performance

L. Jayanthi[1], P. Janardhanan[1], J. Manikandan[2], C. Sivaraj[3] and M. Elango[1*]

[1]Department of Physics, PSG College of Arts and Science, Coimbatore, TN, India
[2]Department of Chemistry, PSG College of Arts and Science, Coimbatore, TN, India
[3]Department of Mathematics, PSG College of Arts and Science, Coimbatore, TN, India
Received: 12.09.2024 Accepted: 29.11.2024 Published: 30.12.2024
*elango@psgcas.ac.in

ABSTRACT

Molybdenum trioxide has emerged as a promising material for various applications due to its semiconducting nature, layered structure, and high redox activity. In this study, we report the preparation, characterization, and electrochemical performance of samarium-doped MoO_3/SiO_2 synthesized via a wet-chemical approach at different pH levels. A comprehensive investigation was carried out to understand the structural, morphological, optical, and electrochemical properties using X-ray diffraction (XRD), field emission scanning electron microscopy (FESEM), transmission electron microscopy (TEM), UV-Vis spectroscopy, Fourier-transform infrared spectroscopy (FTIR), and cyclic voltammetry (CV). The results reveal the impact of pH and samarium doping on the crystallinity, particle morphology, optical bandgap, and charge storage properties of MoO_3. This study highlights the potential of tailored MoO_3-based materials for applications in catalysis, energy storage, and environmental remediation.

Keywords: α-MoO_3/SiO_2 nanoparticles; HRTEM; FTIR; CV studies; Trasatti method.

1. INTRODUCTION

Molybdenum trioxide is an n-type indirect semiconductor with a wide bandgap of 2.8–3.6 eV, known for its excellent thermal and chemical stability, high ionic conductivity, and layered crystalline structure. These properties, coupled with the low cost and environmental friendliness of the material, have made MoO_3 a highly sought-after material in fields such as optics, energy storage, catalysis, and environmental science. The layered structure of MoO_3 enables efficient ion intercalation, making it suitable for applications in gas sensors, lithium-ion batteries (LIBs), and photocatalysis (Janardhanan *et al.* 2024).

Recent advancements in MoO_3 research focus on enhancing its performance through doping and nanostructuring. Incorporating rare-earth elements like samarium introduces new electronic states and defects, improving the optical and electrochemical properties of the material. Moreover, optimizing synthesis parameters, such as pH, further influences the structural and functional behavior of MoO_3 (Kumar *et al.* 2020). This study aims to explore the effects of samarium doping and pH modulation on the properties of MoO_3/SiO_2, with a focus on its structural, morphological, and electrochemical characteristics.

2. PREPARATION PROTOCOL

2.1 Materials

Cetyltrimethylammonium bromide, tetraethyl orthosilicate ammonium molybdate tetrahydrate, samarium acetate, ethanol, and acetone were purchased from Molychem Inc and used as such.

2.2 Synthesis Protocol

Nanodimensional SiO_2 was synthesized *via* the Stöber process, where 1 g of cetyltrimethylammonium bromide (CTAB) was dissolved in a 1:2 ethanol-to-water ratio under stirring. To this solution, 0.8 mL of tetraethyl orthosilicate (TEOS) was added dropwise, and the mixture was stirred for 2 hours until a white precipitate formed. The precipitate was washed with ethanol and water, centrifuged, and dried at 100 °C for 12 hours. The resulting SiO_2 particles were preserved for further use in the synthesis of MoO_3/SiO_2 composites.

Undoped MoO_3 and samarium-doped MoO_3 were prepared using a facile wet-chemical approach. First, 0.3 g of SiO_2 was dispersed in 100 mL of deionized water under constant stirring. Ammonium molybdate tetrahydrate and samarium acetate precursors were added sequentially, followed by the slow addition of nitric acid to the solution. The pH was adjusted to the desired value

(9, 10, or 11) using ammonia as the precipitating agent. The solution was stirred at 85 ℃ for 3 hours and aged for 4 hours at room temperature.

The precipitate obtained was centrifuged, washed thoroughly with acetone and ethanol, and dried at 120 ℃ for 24 hours. Finally, the dried product was calcined at 500 ℃ for 3 hours. This protocol was repeated for samples synthesized at pH 9, 10, and 11. The prepared samples were characterized to understand the influence of pH and doping on their structural and functional properties.

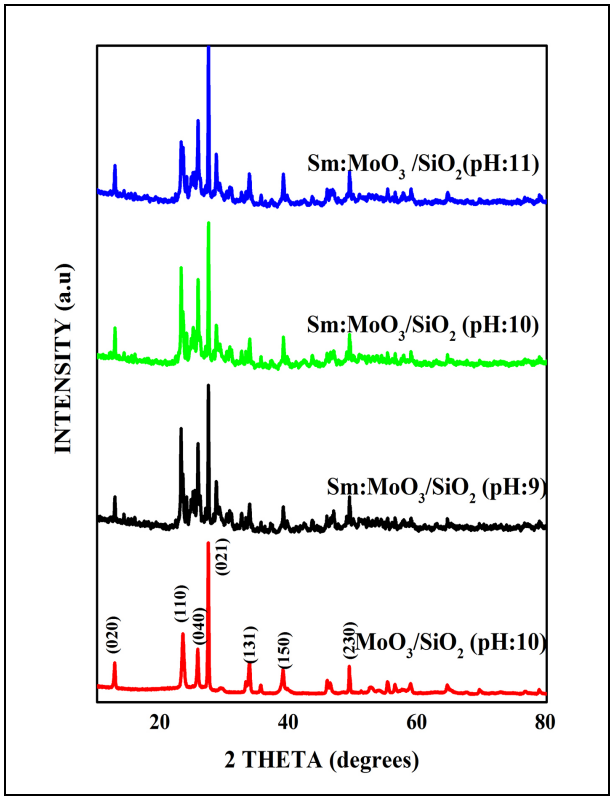

Fig. 1: XRD diffractogram of undoped MoO_3 on SiO_2 and samarium doped MoO_3 on SiO_2 at pH 9.0 10.0 and 11.0

2.3 Characterization Technique

The prepared samples were characterized using a comprehensive tool to examine their structural, textural, surface-chemistry and morphological properties. The structural analysis was done using X-ray diffraction (XRD), high-resolution transmission electron microscopy (HR-TEM). The XRD patterns were obtained with an X'Pert Pro X-ray diffractometer employing a CuK_α anode (λ = 1.5406 Å) operated at 40 KV and a scanning step rate of 0.02°/min. TEM micrographs and selected area electron diffraction (SAED) pattern were captured using JEOL-JEM (2010) microscope to provide the valuable insights into the 3D-morphology, topography, and lattice orientations. Fourier-transform infrared spectral analysis was made using BRUKER Alpha spectrometer employing KBr pellet technique recording a wavelength range of 400-4000 cm^{-1}. Finally, the surface morphology was examined using a TESCAN MIRA-3 scanning electron microscope equipped with an energy-dispersive X-ray (EDX) detector to provide both morphological and compositional data.

3. RESULTS AND DISCUSSION

3.1 XRD Analysis

Fig. 1 depicts the XRD spectra of undoped MoO_3/SiO_2 and samarium-doped MoO_3/SiO_2 samples at varying pH levels revealed significant structural changes. The undoped MoO_3 exhibited sharp peaks characteristic of orthorhombic MoO_3, with prominent planes indexed as (020), (040), and (021). This high crystallinity was indicative of well-ordered structures formed during synthesis (Yang *et al.* 2020).

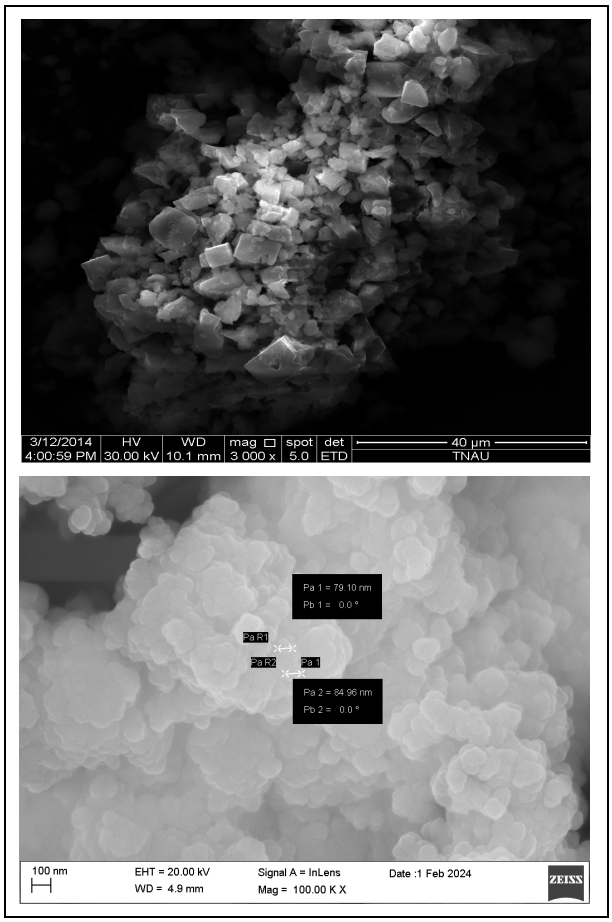

Fig. 2: FESEM image of (a) undoped MoO_3 on SiO_2 b) 9% samarium-doped MoO_3 on SiO_2

For the samarium-doped samples, the diffraction patterns showed reduced peak intensity and increased broadening, especially at higher pH levels. This suggests lattice distortions and smaller crystallite

sizes due to Sm incorporation. The average crystallite size found using the debye scherer formula was 63 nm, 53 nm and 49 nm for the pH 9.0, 10.0 and 11.0 respectively. The crystallite size, calculated using the Debye-Scherrer equation, was found to decrease with increasing pH, indicating enhanced structural disorder. These observations display the role of pH and doping in tailoring the crystalline properties of MoO_3.

3.2 FESEM Analysis

Fig. 2 depicts that the FESEM image (a) of undoped MoO_3/SiO_2 displayed larger, uniformly shaped particles with smooth surfaces and minimal porosity. The morphology of the undoped MoO_3 prepared at optimal conditions reflected a high degree of crystallinity and structural integrity (Zhang and Park 2018).

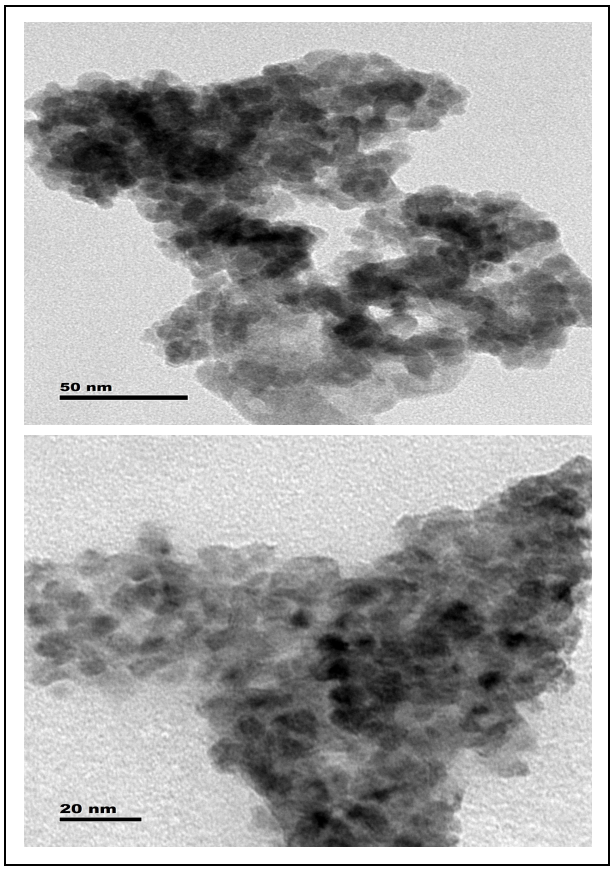

Fig. 3: HRTEM image of (a) undoped MoO_3 on SiO_2 (b) 9% samarium-doped MoO_3 on SiO_2

In contrast, the samarium-doped MoO_3/SiO_2 samples exhibited finer, irregularly shaped particles with increased surface roughness and porosity. The morphological changes were more pronounced at higher pH levels, suggesting that Sm doping and pH modulation significantly influence particle growth and agglomeration. These features enhance the catalytic activity or ion storage properties to be used in environmental remedy.

3.3 TEM Analysis

Fig. 3 shows the HRTEM images of (a) undoped MoO_3 on SiO_2 and (b) Sm doped MoO_3 on SiO_2.TEM images of undoped MoO_3 (Fig. 3a) showed well-defined, compact particles with minimal aggregation, reflecting a uniform crystalline structure. The particle sizes ranged between 50 and 100 nm, consistent with XRD results. Samarium-doped MoO_3 samples (Fig. 3b) displayed smaller, more fragmented particles with irregular shapes. The increased particle agglomeration and reduced size with higher pH indicated significant lattice distortion due to doping. The resulting structural changes enhance the active surface area, which is suitable for applications such as catalysis and energy storage.

3.4 UV Analysis

The UV VIS spectra of the undoped MoO_3 on SiO_2 and Sm doped MoO_3 on SiO_2 is shown in Fig 4. The spectra revealed a redshift in the absorption edge for samarium-doped samples compared to undoped MoO_3. The bandgap energy, estimated using $E_g=1240/\lambda$, was found to decrease with increasing pH. The undoped MoO_3 exhibited a bandgap of ~3.88 eV, while samarium doping reduced the bandgap to ~3.54 eV at pH 11.

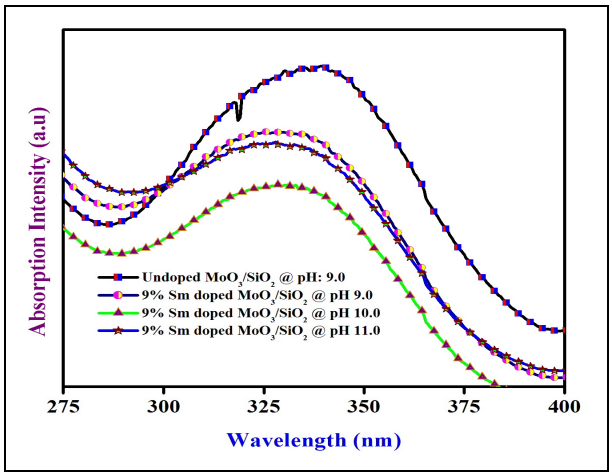

Fig. 4: UV-Vis spectrographs of undoped MoO_3 on SiO_2 and samarium doped MoO_3 on SiO_2 at pH 9.0, 10.0 and 11.0

The reduced bandgap in doped samples highlights the influence of Sm ions in introducing new electronic states and modifying the optical properties. This bandgap narrowing enhances the potential of the material for visible-light-driven photocatalysis and other optoelectronic applications (Vazan *et al.* 2023).

3.5 FTIR Analysis

The FTIR spectra of the undoped MoO_3 on SiO_2 and Sm doped MoO_3 on SiO_2 is portrayed in Fig 5 .The FTIR spectra of undoped MoO_3 displayed characteristic vibrational modes for Mo=O (~970 cm^{-1}) and Mo-O-Mo

(~870 cm^{-1}) bonds, reflecting its orthorhombic structure. These peaks were sharp and well-defined, indicating high structural order.

For samarium-doped MoO_3, these vibrational bands showed a redshift and broadening with increasing pH, suggesting bond elongation and structural distortion due to Sm doping. Additional bands corresponding to Sm-O bonds confirmed the successful incorporation of the dopant into the MoO_3 lattice (Gunasekaran *et al.* 2021).

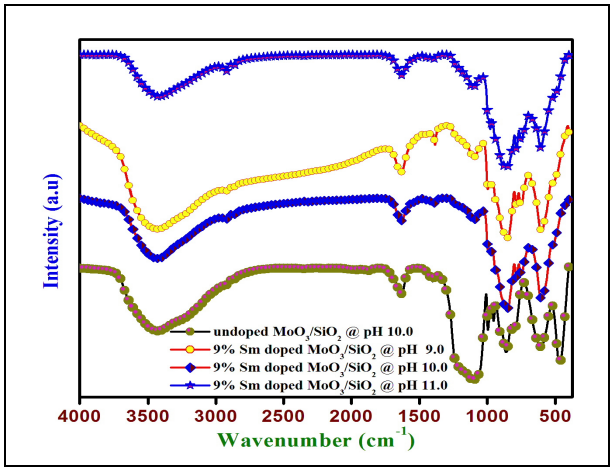

Fig. 5: FTIR spectrographs of undoped MoO_3 on SiO_2 and samarium doped MoO_3 on SiO_2 at pH 9.0 10.0 and 11.0

3.6 CV Analysis

The primary investigations revealed that the Sm doped MoO_3 on SiO_2 processed for optimal characteristics towards efficient super capacitor. The cyclic voltammetry of Sm doped MoO_3 on SiO_2 is shown in Fig. 6. Cyclic voltammetry (CV) curves showed quasi-rectangular profiles, indicative of electric double-layer capacitance (EDLC) behavior. The specific capacitance, calculated from CV data, was highest for samples prepared at pH 11, reflecting superior charge storage properties due to optimal surface morphology and structural integrity (O Concepción and O de Melo 2023).

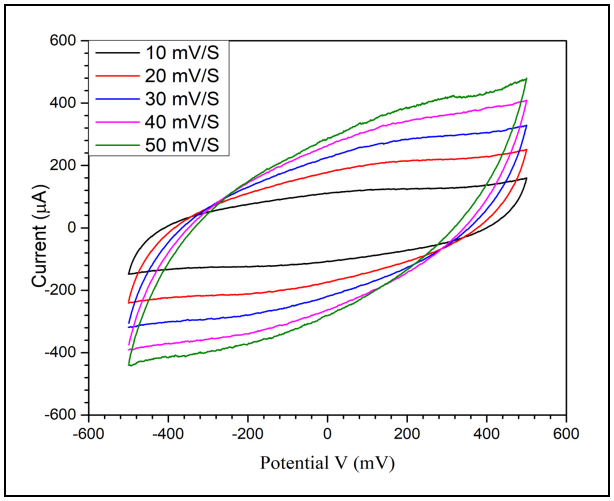

Fig. 6: Cyclic voltametric analysis of Sm doped MoO_3/SiO_2

The specific capacitance is calculated for carious scan rates.

S. No.	Scan rate (mV/S)	Specific capacitance (F/g)
1.	10	22.50
2.	20	17.50
3.	30	15.00
4.	40	12.50
5.	50	10

At higher pH levels, the capacitance decreased, likely due to reduced active surface area and increased structural defects. These findings highlight the critical role of synthesis conditions in optimizing the electrochemical performance of MoO_3-based materials for energy storage applications.

3.7 Trasatti Method

Phenomena of electrochemical storage in an electrode can be measured in various methods. One among such effective method is Trassati method which is governed by two fundamental equations associated with two critical parameters that is the accumulation of charges on the surface of an electrode and the total charge stored at the electrode (capacitance cum diffusion).

These parameters can be determined using the following equations from the Trasatti method:

$$C^*(V) = k_1 v + k v^{\frac{1}{2}}$$

$$\frac{C^*(V)}{v^{\frac{1}{2}}} = k_1 v^{\frac{1}{2}} + k_2$$

Where

$C^*(V)$ - This is the total specific capacitance (or areal capacitance) of the material at a specific potential V.

v - The scan rate of the cyclic voltammetry

k_1- constant related to the contribution of the double-layer capacitance

k - constant related to the contribution of pseudocapacitance

k_2 – A constant that represents the capacitance contribution at v→0

From these equations the k_1 and k_2 indicate the capacity and diffusion control factors.

The Trasatti Analysis was done for CV data of Sm doped MoO_3 at pH 11.

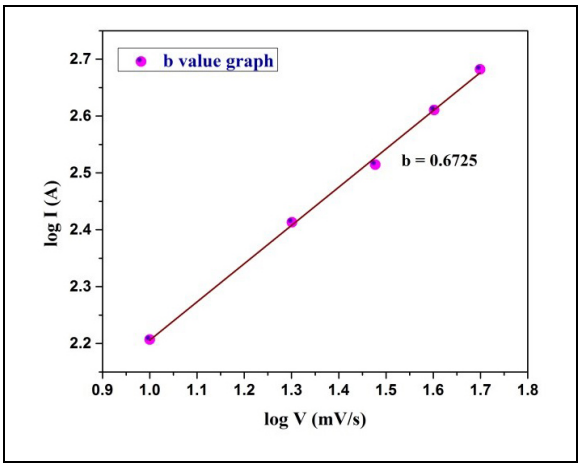

Fig. 7: b-value graph of Sm doped MoO_3/SiO_2

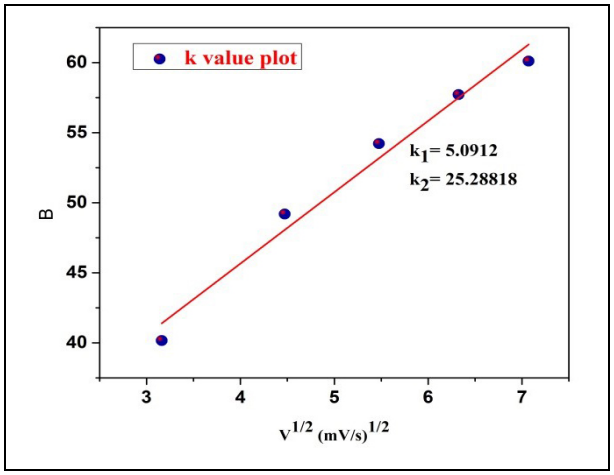

Fig. 8: k-value graph of Sm doped MoO_3/SiO_2

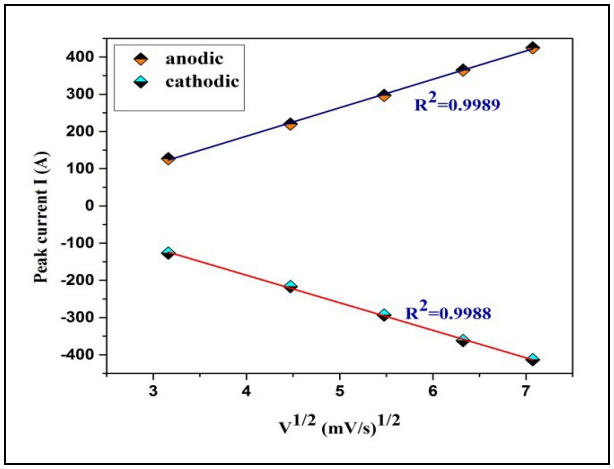

Fig. 9: Reversibility graph of Sm doped MoO_3/SiO_2

Similarly, the value of b gives the information about the type of electrochemical reaction prevails in the charge storing process and if the b- the linear fit slope value is near to 0.5 Faradaic behavior of charging occur in the electrode and if the value of b is close to 1 shows the capacitive nature. From the Fig. 7-9, the b-value for our material is found to be 0.6725, indicating battery-like property. The K value plot that helps in distinguishing between the capacitive and diffusive contributions. More specifically, the reversibility was identified for Sm doped MoO_3/SiO_2 which delivers the R^2 = 0.9989 for anodic peak and R^2 = 0.9988 for cathodic, confirming their excellent reversibility.

4. CONCLUSION

This study demonstrates the significant influence of samarium doping and pH modulation on the structural, optical, and electrochemical properties of MoO_3/SiO_2 composites. The results reveal that pH 11 provides an efficient crystallinity, morphology, and electrochemical performance, making it suitable for energy storage and catalytic applications. Especially the Trassiti method identifies the reversible nature of the materials as an electrode applicant. The findings underscore the potential of doped MoO_3 materials in addressing challenges in energy, environment, and optoelectronics.

REFERENCES

Concepción, O. and de-Melo, O., The versatile family of molybdenum oxides: synthesis, properties, and recent applications, *J. Phys.: Condens. Matter.*, 35, 143002 (2023). https://doi.org/10.1088/1361-648X/acb24a

Gunasekaran, S., Marnadu, R., Thangaraju, D., Chandrasekaran, J., Hegazy, H. H., Somaily, H. H., Durairajan, A., Valente, M. A., Elango, M., Vasudeva, R. and Reddy, M., Development of n-MoO_3@MoS_2/p-Si heterostructure diode using pre-synthesized core@shell nanocomposite for efficient light harvesting detector application, *Mater. Sci. Semicond. Process.*, 135, 106097 (2021). https://doi.org/10.1016/j.mssp.2021.106097

Janardhanan, P., Jayachandran, V., Elango, M. and Manikandan, J., Insights on pH-dependent Physicochemical Properties and Supercapacitance Ability of α-MoO_3, *J. Environ. Nanotechnol.*, 13(3), 09-13 (2024). https://doi.org/10.13074/jent.2024.09.243859

Kumar, S., Singh, A., Singh, R., Singh, S., Kumar, P. and Kumar, R., Facile h-MoO_3 synthesis for NH3 gas sensing application at moderate operating temperature, *Sensor Actuat. B.*, 325, 128974 (2020). https://doi.org/10.1016/j.snb.2020.128974

Vazan, M., Tashkhourian, J. and Haghighi, B., A novel electrochemical sensor based on MoO_3 nanobelt-graphene oxide composite for the simultaneous determination of paracetamol and 4-aminophenol, *Diamond Relat. Mater.*, 140, 110549 (2023). https://doi.org/10.1016/j.diamond.2023.110549

Yang, G., Honglei, Y., Zhang., Xueyao., lqbal., Kanwal., Feng., Fan., Ma., Qin, J., Yuan, J., Cai, F., Ma, Y. and Jiantai, Surfactant-free self-assembly to the synthesis of MoO_3 nanoparticles on mesoporous SiO_2 to form MoO_3/SiO_2 nanosphere networks with excellent oxidative desulfurization catalytic performance, *J. Hazard. Mater.*, 397, 122654 (2020). https://doi.org/10.1016/j.jhazmat.2020.122654

Zhang, Y. and Park, S., Bimetallic AuPd alloy nanoparticles deposited on MoO_3 nanowires for enhanced visible-light driven trichloroethylene degradation, *J. Catal.*, 361, 238-247 (2018). https://doi.org/10.1016/j.jcat.2018.03.010